# REPORT DOCUMENTATION PAGE

Form Approved OMB NO. 0704-0188



| 1. REPORT DATE (DD-MM-YYYY) | 2. REPORT TYPE | 3. DATES COVERED (From - To) |
|---|---|---|
| | New Reprint | - |

4. TITLE AND SUBTITLE

Exothermic surface reactions in alumina–aluminum shell–core nanoparticles with iodine oxide decomposition fragments

5a. CONTRACT NUMBER
W911NF-11-1-0439

5b. GRANT NUMBER

5c. PROGRAM ELEMENT NUMBER
611102

6. AUTHORS
Oliver Mulamba, Michelle Pantoya

5d. PROJECT NUMBER

5e. TASK NUMBER

5f. WORK UNIT NUMBER

7. PERFORMING ORGANIZATION NAMES AND ADDRESSES
Texas Technical University
Box 41035
349 Admin Bldg
Lubbock, TX 79409 -1035

8. PERFORMING ORGANIZATION REPORT NUMBER

9. SPONSORING/MONITORING AGENCY NAME(S) AND ADDRESS (ES)
U.S. Army Research Office
P.O. Box 12211
Research Triangle Park, NC 27709-2211

10. SPONSOR/MONITOR'S ACRONYM(S)
ARO

11. SPONSOR/MONITOR'S REPORT NUMBER(S)
58857-EG.45

12. DISTRIBUTION AVAILIBILITY STATEMENT
Approved for public release; distribution is unlimited.

13. SUPPLEMENTARY NOTES
The views, opinions and/or findings contained in this report are those of the author(s) and should not contrued as an official Department of the Army position, policy or decision, unless so designated by other documentation.

14. ABSTRACT
A pre-ignition reaction (PIR) once thought to be unique to aluminum (Al) and fluorine-based oxidizer reactions is observed for aluminum and an iodine-containing oxidizer. This PIR is exothermic and precedes the main exothermic reaction corresponding to aluminum combustion. For the aluminum and iodine oxide system, exothermic surface chemistry was recently predicted for I-O fragments forming bridge bonds with the alumina passivation shell using first principle calculations, but now has been observed experimentally. Differential scanning calorimetry (DSC) and thermogravimetric analysis (TG) were used to assess aluminum and iodine pentoxide

15. SUBJECT TERMS
differential scanning calorimetry, iodine, aluminum combustion, surface reactions, alumina, exothermic surface chemistry, reaction kinetics

| 16. SECURITY CLASSIFICATION OF: | | | 17. LIMITATION OF ABSTRACT | 15. NUMBER OF PAGES | 19a. NAME OF RESPONSIBLE PERSON |
|---|---|---|---|---|---|
| a. REPORT | b. ABSTRACT | c. THIS PAGE | | | Michelle Pantoya |
| UU | UU | UU | UU | | 19b. TELEPHONE NUMBER 806-742-3563 |

## Report Title

Exothermic surface reactions in alumina–aluminum shell–core nanoparticles with iodine oxide decomposition fragments


## ABSTRACT

A pre-ignition reaction (PIR) once thought to be unique to aluminum (Al) and fluorine-based oxidizer reactions is observed for aluminum and an iodine-containing oxidizer. This PIR is exothermic and precedes the main exothermic reaction corresponding to aluminum combustion. For the aluminum and iodine oxide system, exothermic surface chemistry was recently predicted for I-O fragments forming bridge bonds with the alumina passivation shell using first principle calculations, but now has been observed experimentally. Differential scanning calorimetry (DSC) and thermogravimetric analysis (TG) were used to assess aluminum and iodine pentoxide (I2O5) powder mixtures. Various equivalence ratios were examined and found to affect the PIR onset temperature. Prior to this work, the PIR was attributed solely to surface reactions of the halogen with the Al2O3 surface, but, results shown here indicate that both the alumina surface and aluminum core contribute to a PIR and a minimum activation energy is necessary for PIR production.

# REPORT DOCUMENTATION PAGE (SF298)
# (Continuation Sheet)

Continuation for Block 13

ARO Report Number 58857.45-EG
Exothermic surface reactions in alumina–alumin...

Block 13: Supplementary Note


Approved for public release; distribution is unlimited.

J Nanopart Res (2014) 16:2310
DOI 10.1007/s11051 014 2310 9

RESEARCH PAPER

# Exothermic surface reactions in alumina–aluminum shell–core nanoparticles with iodine oxide decomposition fragments

**Oliver Mulamba · Michelle Pantoya**

Received: 5 November 2013 / Accepted: 30 January 2014


**Abstract** A pre-ignition reaction (PIR) once thought to be unique to aluminum (Al) and fluorine-based oxidizer reactions is observed for aluminum and an iodine-containing oxidizer. This PIR is exothermic and precedes the main exothermic reaction corresponding to aluminum combustion. For the aluminum and iodine oxide system, exothermic surface chemistry was recently predicted for I O fragments forming bridge bonds with the alumina passivation shell using first principle calculations, but now has been observed experimentally. Differential scanning calorimetry (DSC) and thermogravimetric analysis (TG) were used to assess aluminum and iodine pentoxide ($I_2O_5$) powder mixtures. Various equivalence ratios were examined and found to affect the PIR onset temperature. Prior to this work, the PIR was attributed solely to surface reactions of the halogen with the $Al_2O_3$ surface, but, results shown here indicate that both the alumina surface and aluminum core contribute to a PIR and a minimum activation energy is necessary for PIR production.

**Keywords** Aluminum combustion · Pre-ignition reactions · Alumina surface chemistry · Halogen decomposition fragments · Reaction kinetics

O. Mulamba · M. Pantoya (✉)
Mechanical Engineering Department, Texas Tech University, Lubbock, TX 79409 1021, USA
e mail: michelle.pantoya@ttu.edu

## Introduction

The majority of recent interest in halogen-based energetic materials, more specifically iodine-containing formulations, has been motivated by the biocidal effect of iodine and the increasing threats of biological warfare (Clark and Pantoya 2010; Farley and Pantoya 2010; Mulamba et al. 2013). This motivation led to novel findings and potential applications for composites containing iodine (Clark and Pantoya 2010; Zhang et al. 2010; Russell et al. 2011, 2012). Energetic materials containing a mixture of nanoparticles, both fuel and oxidizer, represent a group called metastable intermolecular composites (Miziolek 2002). As the specific surface area of the reactants increases, there is an increase in contact between the fuel and oxidizer particles, which enhances reaction rates and combustion performance (Granier and Pantoya 2004; Bockmon et al. 2005; Plantier et al. 2005). Most of these studies have been performed with aluminum (Al) as the fuel (Kim and Zachariah 2004; Bockmon et al. 2005; Plantier et al. 2005; Dikici et al. 2009; Dreizin 2009). Because Al particles are surrounded by an alumina passivation shell that can range from 2 to 4 nm, the smaller Al particle size leads to increased alumina concentration but significantly increased ignition sensitivity and greater overall reactivity (Aumann et al. 1995; Brown et al. 1998; Dlott 2006; Ahn et al. 2011). Alumina is typically considered a dead weight in propulsion applications because it does not participate in the reaction and acts as a heat sink

Published online: 22 February 2014

(Trunov et al. 2005, 2006; Dikici et al. 2009; Erickson 2010; Gesner et al. 2012). Yet, overall MICs have higher energy densities in comparison to conventional explosives and so have been extensively studied for their potential uses in primers, explosives, and propellants (Kim and Zachariah 2004; Hlavacek et al. 2005; Valliappan et al. 2005). Information and understanding of their reaction kinetics enable tailoring reactants toward a specific application.

The MIC of interest in this work is aluminum (Al) and iodine pentoxide ($I_2O_5$). These composites have been documented to attain flame speeds of up to 2,000 m/s, maximum peak pressures reaching 11 MPa ($m = 0.5$ g), and with a substantially high heat of combustion 6.22 kJ/g in comparison to other thermite reactions such as Al/CuO (4.09 kJ/g), Al/$MoO_3$ (4.72 kJ/g), and Al/$Fe_2O_3$ (3.97 kJ/g) (Dlott 2006; Martirosyan et al. 2009). Farley and Pantoya (2010) found that for heating rates of 10 °C/min, micron-sized particle composites of Al + $I_2O_5$ showed no reaction, while the nanocomposite counterpart produced a complex multistep reaction. The nanoscale particles with increased specific surface area promoted reaction kinetics that otherwise were not detectable with micron scale particles. Molecular dynamic simulations' results (Farley et al. 2013) show a complex multistep reaction, that is, as a result of $I_2O_5$ dissociation fragments that exothermically react with Al and its oxide shell. These fragments including $IO_2$, $IO_3$, and $I_2O_3$ require specific adsorption energies (i.e., −211 kJ/mol per bond) to form bridge bonds with the Al fuel (Farley et al. 2013). These calculations suggest that exothermic surface chemistry in Al + $I_2O_5$ reactions should be observable.

Osborne and Pantoya (2007) studied Al combined with polytetrafluoroethylene (PTFE) and observed a pre-ignition reaction (PIR) associated with the formation of fluorine radicals that react with the $Al_2O_3$ shell at high temperatures, forming as part of its products aluminum fluoride ($AlF_3$). They deduced that the fluorine played a role in the promoting exothermic surface reactions in the $Al_2O_3$ shell. Fluorine and iodine are highly electronegative elements and may exhibit similar halogen-related behaviors when interacting with aluminum particles. The objective of this study is to resolve functional reaction kinetics associated with the Al + $I_2O_5$ system. This will be achieved by characterizing a baseline behavior of the composite and then studying the composite behavior at varying heating rates and equivalence ratios (ERs). With the majority of previous Al + $I_2O_5$ studies using slower heating rates (Clark and Pantoya 2010; Farley and Pantoya 2010; Zhang et al. 2010; Farley et al. 2013) coupled with the predictions of exothermic surface chemistry (Farley and Pantoya 2010), examining higher heating rates may lead to the identification of exothermic surface chemistry. Also, varying ERs allow for an observation of the effects of fuel concentration on the behaviors of these composites and an improved understanding of the composites thermal kinetics.

## Materials and methods

The aluminum (Al) powder was supplied by Nova-Centrix (Austin, TX), with an average particle diameter of 80 nm with 80 % Al purity and 20 % alumina ($Al_2O_3$) passivation shell. The iodine pentoxide ($I_2O_5$) was procured from Sigma Aldrich (St. Louis, MO) at 99 % purity. The Al + $I_2O_5$ mixtures were prepared at varying ERs ranging from 0.8 to 1.2 (i.e., fuel lean to fuel rich). The measured powders were suspended in hexanes and sonicated in a Misonix S3000 sonicator for 1 min cycling 10 s on and 10 s off. The cycling program avoids damage to the oxide shell during this intimate mixing process. Post sonication, the mixtures were poured into a Pyrex® dish and the hexane evaporated while in a fume hood. The mixed powder was then reclaimed for further experimentation.

## Reaction kinetics

Simultaneous thermal analysis (STA) was performed using a Netzsch STA 409 differential scanning calorimeter and thermogravimetric analyzer (DSC/TGA). The samples were programmed to be heated from 30 to 800 °C at a rate of 25 °C/min in an argon environment. Temperature calibrations for the instrument were performed using melting of a set of metal standards resulting in a temperature accuracy of ±1 °C. Platinum crucibles with alumina liners were used and contained 3 mg of sample during testing. Tests were performed in an argon environment where the STA column was evacuated to $1 \times 10^{-4}$ atmospheres using a Pfeiffer model TMU turbo pump and then backfilled and purged with argon at a flow rate of

70 mL $min^{-1}$ for the remainder of the cycle. Sintering can occur during heating and melting, ultimately affecting heat transfer in the DSC measuring head. To insure consistency, repeatability, and minimize artifact alterations of results, three experiments were performed for each sample. The data were analyzed using the NETZSCH Proteus Thermal Analysis software package.

Further, STA experimentation was performed analyzing samples heated to 800 °C at 10, 20, and 40 °C/min. Activation energy was calculated using an isoconversion method presented by Starink (Nixon et al. 2011) and shown in Eq. (1).

$$\ln\left(\frac{B}{T_p^{1.95}}\right) = \frac{E_a}{RT_p} + \ln A \quad (1)$$

From Eq. (1), $B$ is the heating rate, $T_p$ is the exothermic peak temperature, $A$ is a pre-exponential factor, $E_a$ is activation energy, $R$ is the universal gas constant, and $B/T_p^{1.95}$ approximates the reaction rate.

The activation energy $E_a$ (kJ/mol) can be found by plotting ln $(B/T_p^{1.95})$ as a function of $(1/RT_p)$ and taking the slope of the line.

## Results and discussion

The heat flow and mass change results for pure $I_2O_5$ are presented in Fig. 1. The heat flow DSC scale axis is representative of the energy change as a function of temperature and measured in units of mW/mg. The mass loss TG % axis is representative of the mass change as a function of temperature. Mass loss is usually associated with drying, phase change, or gas produced during reaction. Iodine pentoxide is extremely reactive and known to react with moisture in air upon exposure (Farley and Pantoya 2010). Iodic acid, $HIO_3$, is formed as a result and this process is reversed during heating as indicated by the endotherm observed at 200 °C (Farley and Pantoya 2010). The various stages of dissociation are marked on Fig. 1 at the points where the heat flow slope changes (i.e., Stages A D).

The hydroxyl decomposition process can be described by Eq. (2).

$$2HIO_3 \rightarrow H_2O + I_2O_5 \quad (2)$$

The mass loss at ~220 °C coincides with an endotherm, and is indicative of the loss of bonded hydroxyls from $I_2O_5$. There is a slight dip in the heat flow that begins at ~300 °C, corresponding to the initial stages of $I_2O_5$ decomposition. Further $I_2O_5$ decomposition is observed at ~400 °C, where $I_2O_5$ dissociates into the gas phase and 100 % mass loss is observed. As shown in Fig. 1, dissociation for this material is a complex multistage process. It is initiated in Stage A where 70 % of mass is lost and the process is endothermic. This is followed by Stage B where a slight exothermic process causes plateauing in the heat flow, while the mass loss rate remains constant. Stage C shows a sharp endotherm that is exactly coincident with a significant increase in mass loss rate. A substantial change and increase are observed in Stage D representative of an exothermic reaction. This complex process has been previously observed yet it is not well understood or thoroughly explained (Farley and Pantoya 2010). The $I_2O_5$ global decomposition reaction is shown by Eq. (3).

$$I_2O_5 \rightarrow I_2 + 2.5O_2 \quad (3)$$

The elementary reactions and stages in Fig. 1 may be explained using first principles and condensed-phase periodic density functional theory (DFT) analyses performed by Farley et al. (2013). Their simulations analyzed both the gas and solid phases of Al $I_2O_5$ elementary reactions under the assumption Al particles were encapsulated with an $Al_2O_3$ shell and that exothermic interface reactions were taking place upon activation (Farley et al. 2013). Interface adsorption (exothermic) and I-transfer (endothermic) processes were also calculated. Some decomposition kinetics are summarized in Table 1 and can be applied here to explain the exothermic and endothermic behaviors seen in Fig. 1. The reactions in Table 1 where $O_2$ is produced post dissociation are all exothermic and have a negative enthalpy.

The endothermic behavior observed in Stage A of Fig. 1 is associated to the first $I_2O_5$ decomposition stage as shown in Table 1, followed by an exothermic Stage B, endothermic Stage C, and a final exotherm at Stage D.

Figure 2 presents the heat flow (DSC) and mass loss (TG) results for Al + $I_2O_5$ at an ER of 1.0 (i.e., stoichiometric).

Consistent in Figs. 1 and 2, the initial hydroxyl loss at 220 °C is observed as a small endotherm. Following, Fig. 2 presents a small exotherm at ~320 °C, followed by a bigger exotherm at ~405 °C, and then a small endotherm at 450 °C. It is noted that the heat

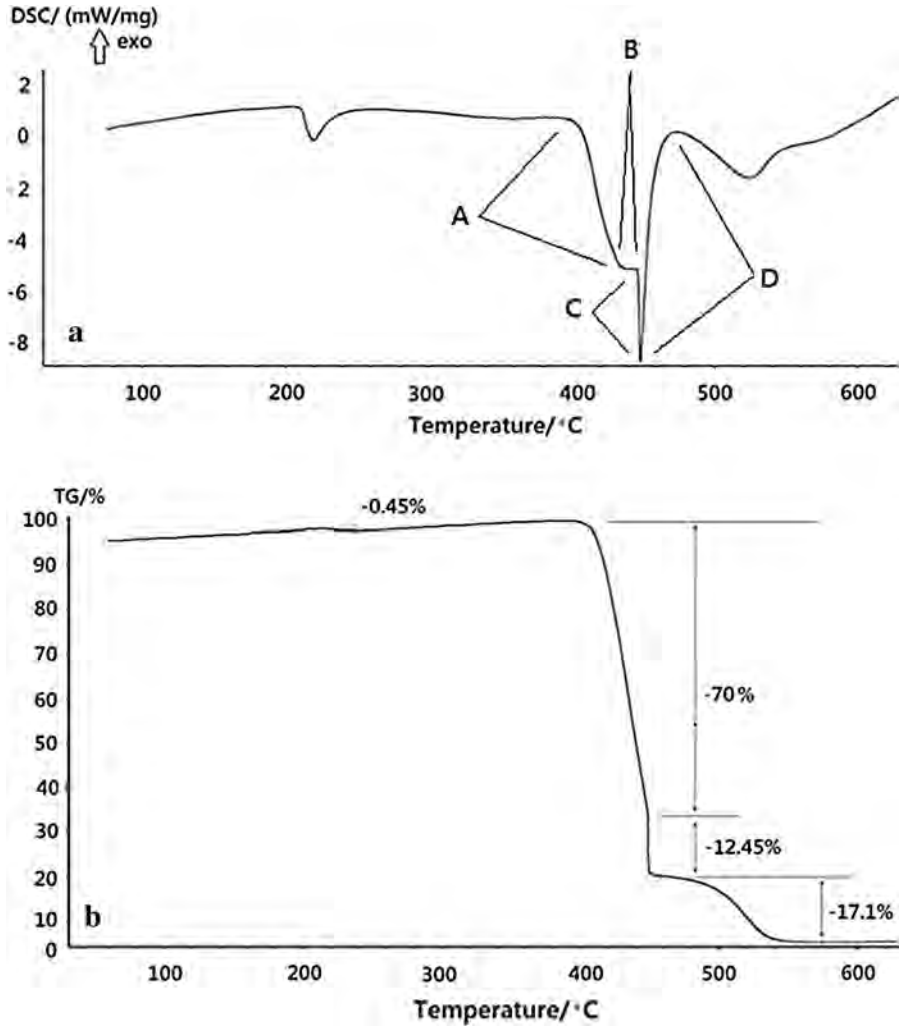


**Fig. 1** Graphs show STA data of pure $I_2O_5$ in an argon environment at a heating rate of 25 °C/min: **a** heat flow reaction stages are marked A D; and, **b** mass loss behavior

flow curves in Figs. 1 and 2 are essentially inverted above 300 °C such that areas showing exotherms in Fig. 1 are showing endotherms in Fig. 2 and vice versa. Therefore, reactions occur at the stages of $I_2O_5$ dissociation. The main exotherm appears to include Stages A B dissociations, while Stages C D correspond to the endotherm and exotherm at ~447 and 450 °C. These reactions all occur below the melting temperature for Al (660 °C) such that Al is in the solid phase. The Al + $I_2O_5$ mass loss pattern in Fig. 2 is similar to the pure $I_2O_5$ mass loss pattern in Fig. 1. Specifically, the initial hydroxyl mass loss is shown at ~220 °C and the changing rates of mass loss between 400 and 500 °C are repeated. All other heat flow behaviors result from adding Al to the mix. For example, a small exotherm occurs at 300 °C where no $I_2O_5$ dissociations were observed. This exotherm resembles an observation by Osborne and Pantoya (2007) who studied fluorine and aluminum. They observed a similar small exotherm prior to the main Al

**Table 1** Dissociation processes reported in (Farley et al. 2013) that correlate with endothermic and exothermic behaviors observed in the $I_2O_5$ STA (i.e., Fig. 1)

| Reaction stage | Dissociation | $\Delta_r H$ (kJ/mol) | Onset temperature |
|---|---|---|---|
| Stage A endotherm | $I_2O_5 \rightarrow IO_2 + IO_3$ | 37.8 | 405 °C |
| Stage B exotherm | $\rightarrow I_2O_3 + O_2$ | 12.0 | 432 °C |
| Stage C endotherm | $\rightarrow IO_2 + IO$ | 23.2 | 447 °C |
| Stage D exotherm | $\rightarrow I_2 + O_2$ | 25.8 | 450 °C |

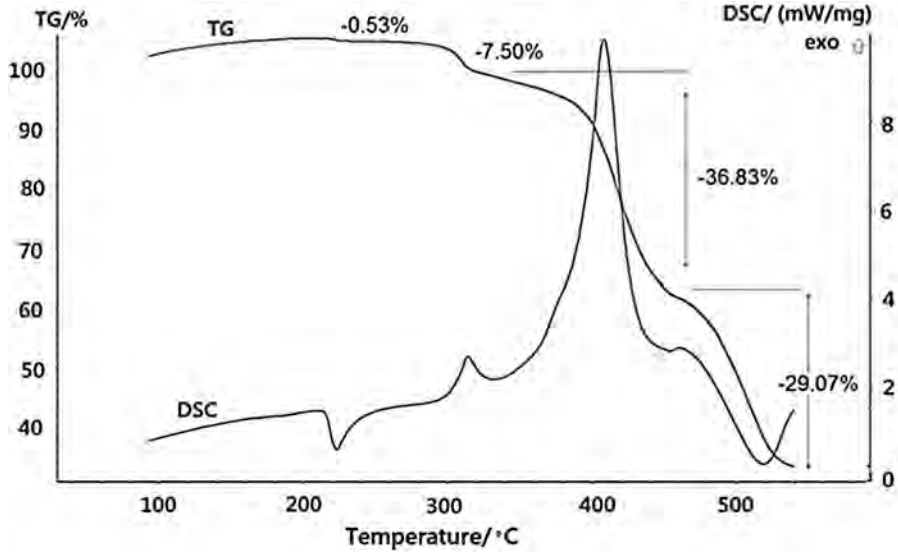


**Fig. 2** Heat flow and mass loss curves from DSC/TG measurements of Al/$I_2O_5$ in an argon environment at a heating rate of 25 °C/min

reaction and coined it a pre-ignition reaction (PIR). They showed that the alumina shell surrounding the Al particle was fluorinated by the fluoride ions from PTFE decomposition, and that this interaction was responsible for the exothermic PIR. The first exotherm shown in Fig. 2 will now be referred to as a PIR exotherm.

This PIR exotherm corresponds to a reaction involving a halogen and is not the main exothermic reaction as indicated by the 2nd exotherm in Fig. 2. In the temperature region of the PIR, $I_2O_5$ has not begun dissociation as shown in Fig. 1; therefore, the PIR exotherm would be a result of kinetics associated with aluminum. Farley et al. (2013) found that $I_2O_5$ and its decomposition fragments adsorb strongly to alumina via bridge bonds and that the adsorption energy is strongly exothermic at 423 kJ/mol for a single $I_2O_5$ molecule. With the adsorption of iodine to $Al_2O_3$, the mass loss observed concurrently with the PIR in Fig. 2 is explained by the oxygen released from $I_2O_5$ dissociation. The adsorption process responsible for the PIR has $I_2O_5$ exothermically dislodging hydroxyls on the $Al_2O_3$ surface and forming I O Al bridge bonds requiring an adsorption energy of 211.495 kJ/mol per bond formed (Farley et al. 2013).

To confirm this PIR behavior associated with $I_2O_5$ fragments reacting with $Al_2O_3$, a mixture of $Al_2O_3$ + $I_2O_5$ was examined for the same conditions as the Al + $I_2O_5$. This analysis isolates reaction between the $Al_2O_3$ shell and $I_2O_5$ and Fig. 3 presents the results.

Figure 3 shows a PIR in the same temperature range as in Al + $I_2O_5$ shown in Fig. 2. Due to the oxygen inertness of $Al_2O_3$ at these temperatures, the exotherm can only be attributed to the bridge bonds forming between $Al_2O_3$ and I O dissociation fragments. Following the PIR, no major exotherm is observed, instead two successive endotherms with the latter being larger than the first. Endothermic behavior in the 420 °C range is consistent with mass loss in all TG figures (Figs. 1b, 2, 3) corresponding to $I_2O_5$ decomposition. As observed in Figs. 1b, 2, and 3, there is a second endotherm attributed to the final stage of mass loss. This second endotherm is much larger in Fig. 3 in comparison to Figs. 1 and 2. The calculated heats of reaction and melting for Figs. 1, 2, and 3 are presented in Table 2.

Trunov et al. (2005) found that the amorphous $Al_2O_3$ shell begins significant growth from 300 °C and then undergoes a phase change from amorphous $Al_2O_3$ to γ $Al_2O_3$ when it reaches critical thickness (∼4 nm) in the 500 550 °C range. This phase change may be responsible for the greater endotherm in Fig. 3 in comparison to Figs. 1 and 2. The higher density associated with γ-$Al_2O_3$ nanocrystallites may promote enhanced bonding behavior (Trunov et al. 2005).

In Fig. 3, one exothermic onset at ∼318 °C is found which coincides with the PIR in Fig. 2 but was not observed in Fig. 1. The element present in composites showing PIR in Figs. 2 and 3 that is not in the composite for Fig. 1 is $Al_2O_3$, such that the PIR is a result of iodination of alumina and the formation

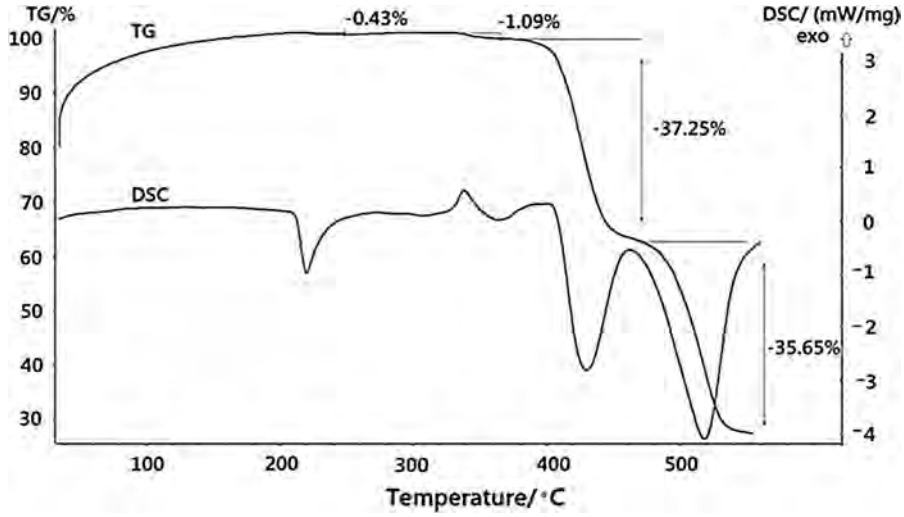


**Fig. 3** Heat flow and mass loss curves from DSC/TG measurements of $Al_2O_3 + I_2O_5$ in an argon environment at a heating rate of 25 °C/min

**Table 2** Quantitative assessment of the heating and melting peaks in Figs. 1, 2, and 3

| | PIR $\Delta_r$ $H$ (J/g) | Main exotherm $\Delta_r$ $H$ (J/g) | 1st endotherm $\Delta_r$ $H$ (J/g) | 2nd endotherm $\Delta_r$ $H$ (J/g) |
|---|---|---|---|---|
| Figure 1 | 0 | 0 | 501 | 106 |
| Figure 2 | 20 | 434 | 0 | 151 |
| Figure 3 | 14 | 0 | 179 | 307 |

of I O Al bonds in coherence with calculations by Farley et al. (2013).

Further experiments were performed for varying ERs to observe an effect on the PIR. A fuel rich 1.2 mixture was studied along with a fuel lean 0.8 mixture, and the heat flow results are presented in Fig. 4.

Figure 4 shows a PIR in all cases. A difference is observed in the onsets of these PIRs: the fuel rich mixture has the lowest onset temperature (i.e., 281.3 °C), while the fuel lean mixture has the highest onset temperature (i.e., 309.1 °C). This leads to a potential concentration-dependent behavior similar to observations by Pantoya and Dean (2009) who found similar correlations between fluorine concentration and PIR onset. The fuel rich mixtures have more Al and, therefore, more $Al_2O_3$ which may allow for increased surface area induced reaction between the alumina shells and $I_2O_5$ leading to earlier observed PIRs. Therefore, there appears to be a concentration factor coupled with the adsorption of $I_2O_5$ dissociating fragments to the $Al_2O_3$ surface that affects the PIR behavior. To investigate how these parameters both play a role the PIR, further testing was performed with a single stoichiometry analyzed at varying heating rates.

A literature search shows that only a couple of heat flow and mass loss studies of $Al + I_2O_5$ has been performed and all did not observe PIR (Farley and Pantoya 2010; Farley et al. 2013). These studies examined heating rates between 2 and 10 °C/min. Therefore, similar tests were performed to extend to higher heating rates at 10, 20, 30, and 40 °C/min and compared with the 25 °C/min results shown in Figs. 1, 2, 3, and 4. Figure 5 presents the results for thermal behavior of $Al + I_2O_5$ at varying heating rates.

Figure 5 shows that no PIR is observed until heating rates $\geq$25 °C/min. If the PIR was simply a matter of $I_2O_5$ fragments interacting with the alumina surface then the lower heating rates would exhibit similar behaviors as the higher heating rates, but that is not observed in Fig. 5. Even though surface interactions contribute to the exothermicity of the PIR (Osborne and Pantoya 2007; Farley and Pantoya 2010; Farley et al. 2013), there appears to be more to the PIR than just surface reactions. The varying parameter in Fig. 5 is the heating rate and so its effects could explain the presence or lack of PIR.

For the varied heating rate, the activation energy was calculated as 1.43 kJ/g [from Eq. (1)] correlated to $Al_2O_3$ and $I_2O_5$ fragments reaction. The activation energy for Al and $I_2O_5$ fragments (main exotherm) was calculated and found to be 1.83 kJ/g and is

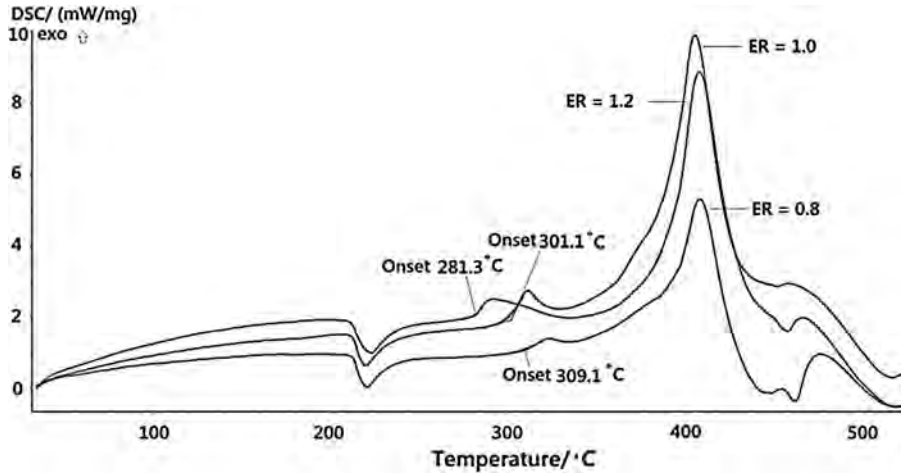


**Fig. 4** Heat flow curves from DSC measurements of Al + $I_2O_5$ in an argon environment at a heating rate of 25 °C/min and for varying equivalence ratios (ER)

comparable to the value obtained by Farley et al. (2013) of 1.79 kJ/g. For diffusion reactions, Al and oxygen species diffuse toward each other through the oxide shell (Rai et al. 2006; Chowdhury et al. 2010). Three forces take part in this action: frictional force (resistance to moving ion), diffusive force (dependent on concentration), and electrostatic force (interaction between ions) (Laidler 1987). The equations describing these forces are presented in (Laidler 1987) and repeated here in Eqs. (4 6).

$$F_{\mathrm{es}} = -\frac{\mathrm{d}U_{\mathrm{es}}}{\mathrm{d}r} \tag{4}$$

$$F_{\mathrm{d}} = -\frac{kT\mathrm{d}c_{\mathrm{B}}}{c_{\mathrm{B}}\mathrm{d}r} \tag{5}$$

$$F_{\mathrm{r}} = -f_{\mathrm{B}}\frac{\mathrm{d}r}{\mathrm{d}t} \tag{6}$$

In these equations, $U_{\mathrm{es}}$ is the electrostatic potential, $c_{\mathrm{B}}$ is the concentration, $f_{\mathrm{B}}$ is the frictional coefficient, $r$ is the depth into the surface, $T$ is the temperature, $k$ is the thermal conductivity, and $\mathrm{d}r/\mathrm{d}t$ is the diffusive velocity (Laidler 1987). These forces are combined to form the diffusive flux ($J_{\mathrm{B}}$) which refers to the number of ions passing through the surface. The equation for $J_{\mathrm{B}}$ is derived in (Laidler 1987) and given by Eq. (7).

$$J_{\mathrm{B}} = \frac{4\pi r^2 kT}{f_{\mathrm{B}}}\left(\frac{\mathrm{d}c_{\mathrm{B}}}{\mathrm{d}r} + \frac{c_{\mathrm{B}}\mathrm{d}U_{\mathrm{es}}}{kT\mathrm{d}r}\right) = -\frac{\mathrm{d}r}{\mathrm{d}t}4\pi r^2 \tag{7}$$

Increasing the heating rate increases the temperature gradient between the outside surface and the core, and higher temperatures cause an increase in molecular kinetic energy represented by Eq. (8).

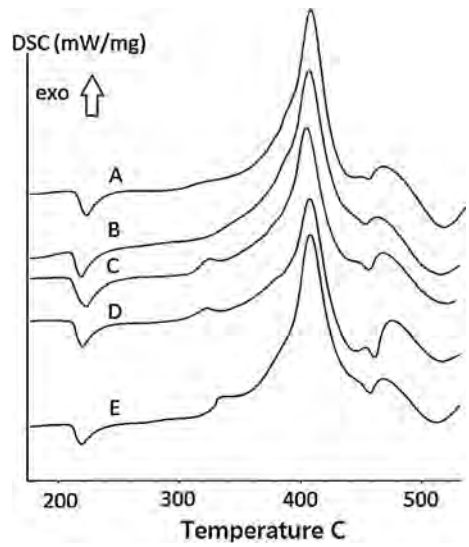


**Fig. 5** The effects of vary heating rates: *A* 10, *B* 20, *C* 25, *D* 30, and *E* 40 °C/min for composite at 0.8 ER examined in an argon environment

$$K_{\mathrm{energy}} = \frac{1}{2}m\left(\frac{\mathrm{d}r}{\mathrm{d}t}\right)^2 \tag{8}$$

Therefore, if heating rate is increased, kinetic energy is increased, and diffusive velocity is increased in accordance with Eq. (6). An increase in diffusive velocity relates to an increase in diffusive flux and promotes increased reaction of iodine and $Al_2O_3$. Based on the deductions above, the electrostatic component of diffusive flux and the ionic nature of this composite, $I_2O_5$ fragments also diffuse into the $Al_2O_3$ shell. Therefore, the $Al_2O_3$ surface is not only

interacting with oxygen and the $I_2O_5$ fragments, but also there is diffusion of oxygen and some ionic $I_2O_5$ fragments into the oxide layer.

Based on Fig. 5 increasing heating rate beyond the threshold where the PIR is observed (i.e., 25 °C/min) results in a consistent PIR observation. For diffusion controlled reactions, increasing heating rates increases diffusion velocities of the oxygen toward the Al and of the Al toward the oxygen, but it also increases the diffusion flux of other ionic elements. Therefore, there appears to be a balance such that beyond a threshold heating rate, the concentration of ionic elements diffusing into the shell would balance the oxygen to Al diffusion and exhibits a consistent PIR. It is also noted that slower heating rates may reach this threshold such that concentration of $I_2O_5$ to $Al_2O_3$ interaction is sufficient for PIR, the reaction may be simultaneous with the main combustion reaction and, therefore, cannot be observed. These observations suggest that not just surface reactions are responsible for the PIR, but core interactions as well.

## Conclusion

Exothermic surface chemistry associated with the alumina passivation shell and iodine-containing species was identified prior to the main aluminum combustion reaction. Powder composites composed of nanoscale aluminum particles passivated with an alumina shell and iodine pentoxide particles were examined using differential scanning calorimetry (DSC) and thermogravimetric analysis (TG). A multistaged endothermic/exothermic behavior unique to $I_2O_5$ was observed and explained using predicted molecular dynamics models that result from multiple $I_2O_5$ dissociation fragments. A PIR once thought to be unique to nano-Al/PTFE mixtures was revealed for the $Al/I_2O_5$ and $Al_2O_3/I_2O_5$ mixtures, as well as fuel rich and fuel lean mixtures. Correlations with the diffusive flux showed that PIR is dependent on both the concentration and activation energy. Adsorption of $I_2O_5$ fragments to the $Al_2O_3$ surface coupled with diffusion of ionic $I_2O_5$ fragments into the $Al_2O_3$ shell was found to play a significant role in the production of PIRs. The effect of varying ERs did not affect the production of a PIR but rather its onset temperature. The fuel rich mixtures show lower onset temperatures and the fuel lean mixtures showed higher onset temperatures such that the PIR was concentration dependent. These are impactful findings because the alumina passivation shell is typically considered dead weight and a heat sink in combustion reactions, but it is shown here to participate exothermically in the reaction when combined with an iodine-containing oxidizer.

**Acknowledgments** The authors gratefully acknowledge support from the Army Research Office under contract W911NF1110439 and encouragement from our Program Manager, Dr. Ralph Anthenien.

## References

Ahn JY, Kim WD, Cho K, Lee D, Kim SH (2011) Effect of metal oxide nanostructures on the explosive property of metastable intermolecular composite particles. Powder Technol 211:65 71

Aumann CE, Skofronick GL, Martin JA (1995) Oxidation behavior of aluminum nanopowders. J Vac Sci Technol B 13:1178 1183

Bockmon BS, Pantoya ML, Son SF, Asay BW, Mang JT (2005) Combustion velocities and propagation mechanisms of metastable interstitial composites. J Appl Phys 98:064903

Brown ME, Taylor SJ, Tribelhorn MJ (1998) Fuel oxidant particle contact in binary pyrotechnic reactions. Propel lants Explos Pyrotech 23:320 327

Chowdhury S, Sullivan K, Piekiel N, Zhou L, Zachariah MR (2010) Diffusive vs explosive reaction at the nanoscale. J Phys Chem C 114:9191 9195

Clark BR, Pantoya ML (2010) The aluminium and iodine pentoxide reaction for the destruction of spore forming bacteria. Phys Chem Chem Phys 12:12653 12657

Dikici B, Dean SW, Pantoya ML, Levitas VI, Jouet RJ (2009) Influence of aluminum passivation on the reaction mechanism: flame propagation studies. Energy Fuels 23:4231 4235

Dlott DD (2006) Thinking big (and small) about energetic materials. Mater Sci Technol 22:463 473

Dreizin EL (2009) Metal based reactive nanomaterials. Prog Energy Combust Sci 35:141 167

Erickson M (2010) Reaction velocities in free standing alumi num and copper oxide thin films. Thesis, University of Central Florida

Farley C, Pantoya M (2010) Reaction kinetics of nanometric aluminum and iodine pentoxide. J Therm Anal Calorim 102:609 613

Farley CW, Pantoya ML, Losada M, Chaudhuri S (2013) Linking molecular level chemistry to macroscopic com bustion behavior for nano energetic materials with halogen containing oxides. J Chem Phys 139:074701 074708

Gesner J, Pantoya ML, Levitas VI (2012) Effect of oxide shell growth on nano aluminum thermite propagation rates. Combust Flame 159:3448 3453

Granier JJ, Pantoya ML (2004) Laser ignition of nanocomposite thermites. Combust Flame 138:373 383

Hlavacek V, Pranda P, Prandova K (2005) Reactivity, stored energy, and dislocations in solid solid reacting systems. Chem Eng Commun 192:933 940

Kim SH, Zachariah MR (2004) Enhancing the rate of energy release from nanoenergetic materials by electrostatically enhanced assembly. Adv Mater 16:1821 1825

Laidler KJ (1987) Chemical kinetics. Pearson Education, Singapore

Martirosyan KS, Wang L, Luss D (2009) Novel nanoenergetic system based on iodine pentoxide. Chem Phys Lett 483: 107 110

Miziolek AW (2002) Nanoenergetics: an emerging technology area of national importance. Adv Mater Manuf Test Inf Anal Cent 6:43

Mulamba O, Hunt EM, Pantoya ML (2013) Neutralizing bac terial spores using halogenated energetic reactions. Bio technol Bioprocess Eng 18:918 925

Nixon E, Pantoya ML, Sivakumar G, Vijayasai A, Dallas T (2011) Effect of a superhydrophobic coating on the com bustion of aluminium and iron oxide nanothermites. Surf Coat Technol 205:5103 5108

Osborne DT, Pantoya ML (2007) Effect of al particle size on the thermal degradation of Al/Teflon mixtures. Combust Sci Technol 179:1467 1480

Pantoya ML, Dean SW (2009) The influence of alumina pas sivation on nano Al/Teflon reactions. Thermochim Acta 493:109 110

Plantier KB, Pantoya ML, Gash AE (2005) Combustion wave speeds of nanocomposite Al/Fe2O3: the effects of Fe2O3 particle synthesis technique. Combust Flame 140:299 309

Rai A, Park K, Zhou L, Zachariah MR (2006) Understanding the mechanism of aluminium nanoparticle oxidation. Combust Theory Model 10:843 859

Russell R, Bless S, Pantoya M (2011) Impact driven thermite reactions with iodine pentoxide and silver oxide. J Energ Mater 29:175 192

Russell R, Bless S, Blinkova A, Chen T (2012) Sporicidal effects of iodine oxide thermite reaction products. In: Elert ML, Buttler WT, Borg JP, Jordan JL, Vogler TJ (eds) Shock compression of condensed matter 2011, Pts 1 and 2, vol 1426

Trunov MA, Schoenitz M, Zhu X, Dreizin EL (2005) Effect of polymorphic phase transformations in Al2O3 film on oxi dation kinetics of aluminum powders. Combust Flame 140: 310 318

Trunov MA, Umbrajkar SM, Schoenitz M, Mang JT, Dreizin EL (2006) Oxidation and melting of aluminum nanopowders. J Phys Chem B 110:13094 13099

Valliappan S, Swiatkiewicz J, Puszynski JA (2005) Reactivity of aluminum nanopowders with metal oxides. Powder Technol 156:164 169

Zhang S, Schoenitz M, Dreizin EL (2010) Iodine release, oxi dation, and ignition of mechanically alloyed Al I com posites. J Phys Chem C 114:19653 19659